J. Fluid Mech. (2007), *vol.* 571, *pp.* 265–280.
doi:10.1017/S0022112006002965 Printed in the United Kingdom

Steady streaming in a turbulent oscillating boundary layer

By PIETRO SCANDURA

Department of Civil and Environmental Engineering, University of Catania, Viale A. Doria, 6, Catania 95125, Italy

(Received 4 January 2006 and in revised form 11 July 2006)

The turbulent flow generated by an oscillating pressure gradient close to an infinite plate is studied by means of numerical simulations of the Navier–Stokes equations to analyse the characteristics of the steady streaming generated within the boundary layer. When the pressure gradient that drives the flow is given by a single harmonic component, the time average over a cycle of the flow rate in the boundary layer takes both positive and negative values and the steady streaming computed by averaging the flow over n cycles tends to zero as n tends to infinity. On the other hand, when the pressure gradient is given by the sum of two harmonic components, with angular frequencies ω_1 and $\omega_2 = 2\omega_1$, the time average over a cycle of the flow rate does not change sign. In this case steady streaming is generated within the boundary layer and it persists in the irrotational region. It is shown both theoretically and numerically that in spite of the presence of steady streaming, the time average over n cycles of the hydrodynamic force, acting per unit area of the plate, vanishes as n tends to infinity.

1. Introduction

Oscillating boundary layers have attracted the attention of many researchers because of their importance in many phenomena of both scientific and engineering interest, such as water wave propagation, unsteady flows in pipes and biological flows. The wall boundary layer driven by a sinusoidally oscillating pressure gradient (Stokes boundary layer) has been studied experimentally by Hino, Sawamoto & Takasu (1976), Hino *et al.* (1983), Jensen, Sumer & Fredsøe (1989), Eckmann & Grotberg (1991), Akhavan, Kamm & Shapiro (1991*a*), Lodahl, Sumer & Fredsøe (1998). Various theoretical works such as von Kerczek & Davis (1974), Hall (1978), Cowley (1987), Wu (1992), Hall (2003), Blennerhassett & Bassom (2006) have addressed the stability of the Stokes layer. The Stokes boundary layer has also been studied numerically by Spalart & Baldwin (1987), Akhavan, Kamm & Shapiro (1991*b*), Vittori & Verzicco (1998), Costamagna, Vittori & Blondeaux (2003). Herein the Reynolds number R_δ of the Stokes boundary layer is defined as $R_\delta = U_0^* \sqrt{2\nu^*/\omega^*}/\nu^*$, where U_0^* and ω^* are the amplitude and the angular frequency of velocity oscillations far from the wall and ν^* is the kinematic viscosity of the fluid. The length $\delta^* = \sqrt{2\nu^*/\omega^*}$ is the conventional thickness of the Stokes boundary layer.

On the basis of the results reported in the literature, as the value of the Reynolds number increases, the flow in the Stokes boundary layer goes through four regimes: (i) for low Reynolds numbers the flow is laminar and unidirectional and is described by the well-known Stokes solution (Stokes 1851); (ii) for R_δ larger than about 100 the disturbed laminar regime begins, where small perturbations are observed, but the

flow remains similar to the Stokes solution; (iii) when the Reynolds number becomes larger than about 550 the flow is in the intermittently turbulent regime in which the perturbations grow and turbulent bursts appear during the decelerating phase of the cycle; the flow is thus significantly different from the Stokes solution; (iv) for Reynolds number larger than about 3500 the flow is in the fully developed turbulent regime (Jensen *et al.* 1989) where turbulence is present throughout the cycle.

An interesting phenomenon that often appears in oscillating boundary layers is the generation of steady streaming (see Riley 2001 for a broad review on the subject). Rayleigh (1883) was the first to study the generation of steady streaming in a flow dominated by an oscillatory velocity component. In particular, he analysed the mechanism by which an acoustic wave in a closed duct induces steady streaming and determined the Eulerian drift in the wall boundary layer. The presence of steady streaming directed shoreward in the laminar oscillating boundary layer at the bottom of a sea wave propagating over a plane bed was demonstrated by Longuet-Higgins (1953). According to the theory developed by him, the steady streaming velocity $\overline{u^*_\infty}$ far from the bottom satisfies the relation $\overline{u^*_\infty} c^*/U_0^{*2} = 0.75$, where c^* is the wave speed. The Longuet-Higgins steady streaming arises because the spatial variability of the flow characteristics in the wave bottom boundary layer generates nonlinear interactions which produce a period-averaged velocity component. The experimental observations of Russel & Osorio (1958) have confirmed the theoretical finding of Longuet-Higgins (1953) for waves of small amplitude propagating over a flat smooth bed and characterized by a laminar bottom boundary layer. In an appendix to the paper of Russel & Osorio (1958), Longuet-Higgins (1958) showed that if the eddy viscosity in a turbulent boundary layer is considered independent of time, the steady streaming velocity at the edge of the boundary layer takes the same value as in the laminar flow. The theory of Longuet-Higgins (1958) agrees with the experiments of Russel & Osorio (1958) but in the latter the flow was probably in the disturbed laminar regime as the Reynolds number was relatively low. Subsequent experimental works of Brebner, Askew & Law (1966), Bijker, Kalkwijk & Picters (1974) and Van Doorn (1981) have indeed shown that the steady streaming velocity at the edge of a turbulent boundary layer is smaller than the value determined by Longuet-Higgins (1958). Moreover, in some shallow depth experiments, an offshore directed (i.e. in the direction opposite to that of the wave propagation) steady streaming has been observed.

In a turbulent wave bottom boundary layer an offshore directed steady streaming also arises because of the wave asymmetry. The underlying mechanism that generates steady streaming when the wave is asymmetric is due to the different characteristics of turbulence during the seaward and landward half-cycles. The steady streaming generated by the wave asymmetry is opposite to the Longuet-Higgins steady streaming, thus explaining why the direction of the steady streaming in a turbulent wave boundary layer may be opposite to that of the wave propagation. The asymmetry-wave steady streaming has been much less studied in the literature, probably because it poses a mathematical problem whose solution cannot be tackled by analytical means. Both the Longuet-Higgins and the asymmetry-wave steady streamings are very important in cross-shore sediment transport by waves.

In order to understand the hydrodynamic processes involved in the generation of steady streaming in a turbulent wave boundary layer, the two mechanisms described above should be analysed separately first and then their interaction considered. The aim of the present work is to study the steady streaming generated in a turbulent oscillating boundary layer because of the wave asymmetry.

Asymmetric waves free from the Longuet-Higgins steady streaming cannot normally be produced in a laboratory. However, the effects of the wave asymmetry can be analysed by using an oscillating water tunnel as in the experiments of Ribberink & Al-Salem (1995). A spatially uniform oscillating boundary layer free from the Longuet-Higgins steady streaming can be generated by using such a device. The work of Ribberink & Al-Salem (1995) was mostly devoted to the study of sediment transport under sheet flow conditions and very few results were provided about the steady streaming induced by the wave asymmetry. The above authors reported that, under asymmetric flow conditions, a net wave-averaged horizontal velocity was measured against the direction of the 'wave propagation', or in the direction of the flow during the trough half-cycle, which was about 4 % of the time-dependent flow velocity.

The effect of the wave asymmetry on the hydrodynamics of the wave bottom boundary layer has been introduced into Reynolds-averaged Navier–Stokes equations models by Trowbridge & Madsen (1984) and Jacobs (1984). The results of these studies qualitatively agree with the previously cited experimental works. In particular, for long waves in shallow depth the Trowbridge & Madsen (1984) model predicts steady streaming in the direction opposite to that of the wave propagation.

Notwithstanding the works mentioned above, to the author's knowledge, no systematic studies have so far been performed, either experimentally or by numerical simulation of the Navier–Stokes equations, on the steady streaming driven by asymmetric flow conditions in a turbulent Stokes layer. Since such a flow is the prototype of the oscillating turbulent boundary layers which are a common feature of various environmental phenomena and applications, an improved understanding of the characteristics of the steady streaming and of the mechanisms by which it is generated would be highly desirable.

The paper is organized as follows. In § 2 the problem is formulated and the numerical approach is briefly described. In § 3 the average flow quantities are introduced and a preliminary insight is given into the mechanism that generates the steady streaming. In § 4 the results of the simulations are reported and discussed. The conclusions are drawn in § 5.

2. Formulation of the problem and numerical approach

We consider the oscillating flow of an incompressible Newtonian fluid generated by a spatially constant pressure gradient close to an infinite plate. Hereinafter a star is used to denote dimensional quantities. As a reference, we introduce a Cartesian coordinate system with the x_1^*- and x_3^*-axes lying on the plate and directed along the streamwise and the spanwise directions respectively and the x_2^*-axis (cross-stream direction) orthogonal to the plate and directed upwards. We assume that at the edge of the boundary layer the flow oscillates according to the wave bottom velocity given by the second-order approximation of the Stokes irrotational wave theory (see Dean & Dalrymple 2000):

$$u_1^* = U_0^* \cos(\omega^* t^*) + U_1^* \cos(2\omega^* t^*), \qquad u_2^* = u_3^* = 0, \tag{2.1}$$

where U_0^* and U_1^* are the amplitudes of velocity oscillations of the first and second harmonic components respectively and t^* is the time. The velocity oscillations given by equation (2.1) are asymmetric, due to the presence of two harmonic components characterized by angular frequencies ω^* and $2\omega^*$. The ratio $u_r = U_1^*/U_0^*$ represents a measure of the wave asymmetry. It is easily to show that in order to match the velocities (2.1), the pressure gradient that drives the flow must have the following

form:

$$\left(\frac{\partial P^*}{\partial x_1^*}, \frac{\partial P^*}{\partial x_2^*}, \frac{\partial P^*}{\partial x_3^*}\right) = (-\varrho^* U_0^* \omega^* \sin(\omega^* t^*) - 2\varrho^* U_1^* \omega^* \sin(2\omega^* t^*), 0, 0), \tag{2.2}$$

where ϱ^* is the fluid density. In order to trigger transition to turbulence, the wall is not perfectly flat and its profile is described by the superimposition of two sinusoidal functions,

$$x_2^* = \eta^*(x_1^*, x_3^*) = h^*[a_{x_1} \cos(\alpha^* x_1^*) + a_{x_3} \cos(\gamma^* x_3^*)]. \tag{2.3}$$

In (2.3), $h^* a_{x_i}$ $(i = 1, 3)$ are the amplitudes of the sinusoidal components, and α^* and γ^* are the wavenumbers in the x_1^*- and x_3^*-directions respectively. After the turbulence has developed, the run is stopped, h^* is set to zero and the simulation is continued on a perfectly flat wall. Generally, two periods are sufficient to get a developed turbulent regime.

The problem is formulated in dimensionless form by introducing the following dimensionless variables:

$$t = t^* \omega^*, \quad (x_1, x_2, x_3) = \frac{x_1^*, x_2^*, x_3^*}{\delta^*}, \quad (u_1, u_2, u_3) = \frac{u_1^*, u_2^*, u_3^*}{U_0^*}, \quad p = \frac{p^*}{\varrho^* U_0^{*2}}. \tag{2.4}$$

In (2.4) u_1^*, u_2^* and u_3^* are the velocity components along the x_1^*-, x_2^*- and x_3^*-directions respectively, and p^* is the pressure. The present flow is characterized by two dimensionless parameters, namely the Reynolds number $R_\delta = U_0^* \delta^* / \nu^*$ and the ratio $u_r = U_1^* / U_0^*$.

The flow is studied by direct numerical simulations of the Navier–Stokes equations in a domain of size L_{x_1}, L_{x_2} and L_{x_3} in the streamwise, cross-stream and spanwise directions respectively. On the plate the no-slip condition is introduced,

$$(u_1, u_2, u_3) = 0 \quad \text{at} \quad x_2 = \eta(x_1, x_3). \tag{2.5}$$

Since the amplitudes of the wall waviness are assumed to be much smaller than the thickness of the boundary layer ($h = h^*/\delta^* \ll 1$), the condition (2.5) can be enforced by using the procedure outlined in Vittori & Verzicco (1998),

$$(u_1, u_2, u_3) = -\eta(x_1, x_3) \frac{\partial (u_1, u_2, u_3)}{\partial x_2}\bigg|_{x_2=0} + O(h^2) \quad \text{at} \quad x_2 = 0. \tag{2.6}$$

When L_{x_2} is large enough that the vorticity does not propagate to $x_2 = L_{x_2}$, close to the upper boundary of the computational domain the flow remains irrotational and the velocity components (u_1, u_2, u_3) oscillate as $(\cos(t) + u_r \cos(2t), 0, 0)$. Therefore, the following boundary condition is introduced at $x_2 = L_{x_2}$:

$$\frac{\partial}{\partial x_2}(u_1, u_3) = u_2 = 0 \quad \text{at} \quad x_2 = L_{x_2}, \tag{2.7}$$

which is equivalent to imposing the vanishing of the tangential stresses. Condition (2.7) can be considered as a symmetry boundary condition because it is equivalent to introducing a mirror flow field with respect to the $x_2 = L_{x_2}$ plane.

Finally, the flow is assumed to be homogeneous along the x_1- and x_3-directions, i.e. along these directions the turbulence is statistically invariant under translation; thus periodic boundary conditions are introduced along the x_1- and x_3-axes. Unless otherwise stated, in all the simulations a wavy wall, characterized by $h = h^*/\delta^* = 5 \times 10^{-4}$, $a_{x_1} = 1$, $a_{x_3} = 0.1$, $\alpha = \alpha^* \delta^* = 4\pi / L_{x_1}$ and $\gamma = \gamma^* \delta^* = 4\pi / L_{x_3}$ is introduced.

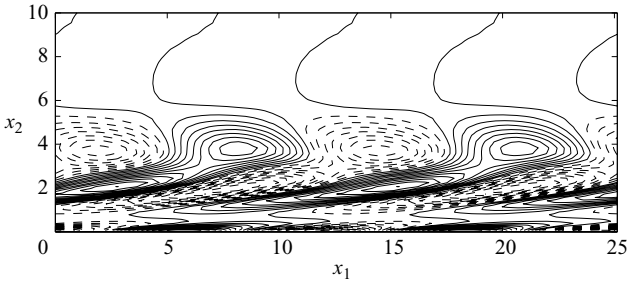

FIGURE 1. Contour plot of the spanwise vorticity component Ω_3 in the plane $x_3 = 5.9$ for $h = 0.005$, $R_\delta = 500$, $u_r = 0$; $\Delta\Omega_3 = 0.002$; continuous line: positive vorticity, dashed line: negative vorticity.

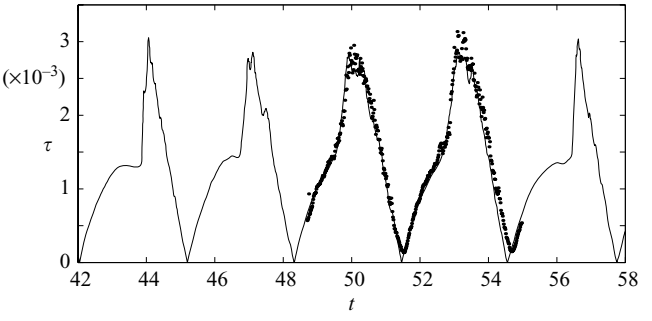

FIGURE 2. Time development of wall shear stress for $R_\delta = 1120$ and $u_r = 0$; continuous line: numerical results; dots: experimental measurements of Jensen *et al.* (1989).

The numerical procedure adopted makes use of centred second-order finite differences on a staggered grid to approximate the spatial derivatives. The time advancement of the governing equations employs a fractional step method described by, among others, Kim & Moin (1985) and Rai & Moin (1991). The convective terms are evaluated explicitly by a three-step Runge–Kutta scheme (Rai & Moin 1991) while the viscous terms are evaluated implicitly by the Crank–Nicholson scheme.

In order to show the reliability and the correctness of the numerical code, two simulations have been performed and the results have been compared with previous numerical solutions and experimental measurements. Vittori & Verzicco (1998) simulated the disturbed laminar regime for $R_\delta = 500$ and $u_r = 0$. It is known that in this regime the perturbations to the laminar behaviour (Stokes solution) are generated by wall imperfections or by other types of disturbances (Costamagna *et al.* 2003). Therefore, as a source of disturbances Vittori & Verzicco (1998) introduced a wavy wall described by equation (2.3) with $h = 5 \times 10^{-3}$, $a_{x_1} = 1$, $a_{x_3} = 0.1$, $\alpha = 0.5$ and $\gamma = 1$. They fixed the dimensions of the computational domain as $L_{x_1} = L_{x_2} = 25.13$, $L_{x_3} = 12.57$ and used a grid with 64, 64 and 32 gridpoints in the x_1-, x_2- and x_3-directions respectively. In figure 1 contour plot of the spanwise vorticity component Ω_3 is shown in a vertical plane at $t = 25.13$. The vorticity has been computed after the average in the x_1-direction of the velocity field has been removed. There is good agreement between the present results and those shown in figure 5(*c*) of Vittori & Verzicco (1998).

A further check of the numerical code has been carried out on test 7 of Jensen *et al.* (1989) ($R_\delta = 1120$). The computed wall shear stress $\tau = \tau^*/\varrho U_0^{*2}$ averaged over the plate is compared with that measured experimentally in figure 2. The size of

the computational domain is the same as in the previous case and 120, 120 and 80 gridpoints have been introduced in the x_1-, x_2- and x_3-directions respectively. The results show that the turbulent flow field is adequately resolved by the numerical code.

3. Average flow quantities

In order to analyse the results, we introduce the period average f_{pa} and the steady component $\bar{f}$ of a flow quantity f as

$$f_{pa}(i) = \frac{1}{T}\int_{(i-1)T}^{iT} f(t)\,\mathrm{d}t, \quad \bar{f} = \lim_{n\to\infty}\frac{1}{nT}\int_0^{nT} f(t)\,\mathrm{d}t, \tag{3.1}$$

where n is an integer, $T = 2\pi$ is the dimensionless period of the oscillating pressure gradient and i is an integer used to denote the generic cycle. It can be shown that the following equations hold:

$$\bar{f} = \lim_{n\to\infty}\frac{1}{n}\sum_{i=1}^{n} f_{pa}(i) = \langle f(t)\rangle_{pa}, \tag{3.2}$$

where $\langle f(t)\rangle$ is the ensemble average of f defined as an average performed over an infinite number of flow realizations. By assuming the ergodic hypothesis (Monin & Yaglom 1971), the ensemble average can be substituted by a time average in stationary turbulence and by a spatial average in homogeneous turbulence. In the present case the ensemble average is approximated by performing a spatial average along the homogeneous directions and a phase average. As the present flow is homogeneous both in the x_1- and in the x_3-directions, $\langle f(t)\rangle$ and $\bar{f}$ are constant on $x_2 = \text{const}$ planes. Some insight into the physical mechanism that drives the steady current can be gained from the Navier–Stokes equations. First, let us take the ensemble average of the Navier–Stokes equation in the streamwise direction and then the period average, taking into account that the period average of the pressure gradient (2.2) is equal to zero and that the flow is homogeneous both in the x_1- and x_3-directions,

$$R_\delta\frac{\partial\langle u_1'u_2'\rangle_{pa}}{\partial x_2} = \frac{\partial^2\langle u_1\rangle_{pa}}{\partial x_2^2}, \tag{3.3}$$

where $u_1' = u_1 - \langle u_1\rangle$ and $u_2' = u_2 - \langle u_2\rangle$. Then, by integrating (3.3) between 0 and x_2 and taking into account that the Reynolds stress vanishes at $x_2 = 0$,

$$R_\delta\langle u_1'u_2'\rangle_{pa} = \frac{\partial\overline{u_1}}{\partial x_2} - \left.\frac{\partial\overline{u_1}}{\partial x_2}\right|_{x_2=0}, \tag{3.4}$$

where the equality $\langle u_1\rangle_{pa} = \overline{u_1}$ has been used. Far from the wall, where the flow is irrotational, both the left-hand side and the first term on the right-hand side of (3.4) are equal to zero; then $(\partial\overline{u_1}/\partial x_2)|_{x_2=0} = 0$. This result implies that the steady component of the hydrodynamic force acting on the plate vanishes. A further integration of (3.4) shows that

$$\overline{u_1} = R_\delta\int_0^{x_2}\langle u_1'u_2'\rangle_{pa}\,\mathrm{d}x_2. \tag{3.5}$$

From equation (3.5), it is clear that the steady streaming is forced by the period average of the Reynolds stress $\langle u_1'u_2'\rangle$.

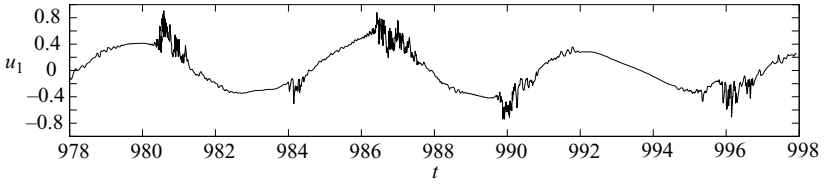

FIGURE 3. Time development of the velocity component u_1 at $(x_1,\ x_2,\ x_3) = (2.26,\ 0.28,\ 1.77)$ for $R_\delta = 800$ and $u_r = 0$.

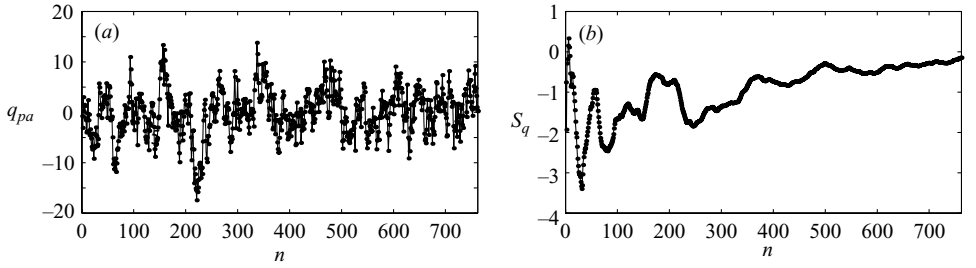

FIGURE 4. (*a*) Period average of the flow rate. (*b*) Trend of the series S_q. $R_\delta = 800$, $u_r = 0$.

4. Discussion of the results

In the present investigation we consider values of the flow parameters that fall in the intermittently turbulent regime (Vittori & Verzicco 1998). A first simulation is performed by fixing $R_\delta = 800$ and $u_r = 0$. The size of the computational domain is $L_{x_1} = L_{x_2} = 25.13$ and $L_{x_3} = 12.57$. Such values of L_{x_1}, L_{x_2} and L_{x_3} are equal to those used by Vittori & Verzicco (1998) who verified that no important changes in the turbulent characteristics take place when the dimensions L_{x_1} and L_{x_3} are doubled. They also showed that the averaged quantities computed with these domain dimensions show an acceptable agreement with the experimental measurements. Vittori & Verzicco (1998) did not investigate how the results change when the value of L_{x_2} is increased. However, a value of 25.13 for L_{x_2} is large enough for an irrotational region to be set up in the upper part of the computational domain (see the discussion that leads to (2.7)). Thus, an increase of L_{x_2} does not affect the turbulence characteristics.

A grid with 100, 100 and 64 gridpoints in the streamwise, cross-stream and spanwise directions respectively is employed to solve the governing equations. The appropriate resolution of the smallest vortices obtained by means of this numerical grid is demonstrated in Costamagna *et al.* (2003), where the power spectra are shown to be characterized by an acceptable drop-off both in the x_1- and in the x_3-directions even with a $64 \times 64 \times 32$ numerical grid. In figure 3 the time development of the velocity component u_1 at $(x_1,\ x_2,\ x_3) = (2.26,\ 0.28,\ 1.77)$ is plotted. The qualitative behaviour of the velocity is similar to that observed by Hino *et al.* (1976) and by Vittori & Verzicco (1998). Turbulence appears explosively around the end of the accelerating phase and persists during the first part of the decelerating phase, and during the following accelerating phase the flow recovers a laminar-like behaviour. The period average q_{pa} of the flow rate q ($q = \int_0^{L_{x_2}} \int_0^{L_{x_3}} u_1 \, \mathrm{d}x_2 \, \mathrm{d}x_3$) takes non-zero values, as shown in figure 4(*a*), where q_{pa} is plotted versus the number n of the cycle. The period average of the flow rate changes from cycle to cycle and takes both positive and negative values.

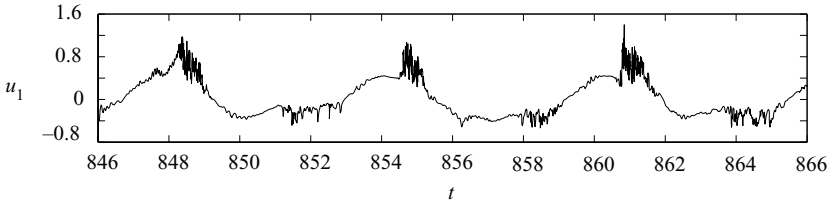

FIGURE 5. Time development of the velocity component u_1 at $(x_1,\ x_2,\ x_3) = (2.26,\ 0.28,\ 1.77)$ for $R_\delta = 800$ and $u_r = 0.3$.

The presence of values of q_{pa} different from zero in a flow that is driven by a sinusoidally oscillating pressure gradient is due to the nonlinear terms of the governing equations, which cause the flow during a half-cycle not to be the mirror image of that during the following half-cycle. This phenomenon can be observed by looking at figure 3: the turbulent velocity fluctuations which appear during the first half-cycle ($980.17 < t \leqslant 983.32$) are stronger and pervade a larger part of the cycle than those which are present during the second one ($983.32 < t \leqslant 986.46$). Furthermore, the disappearance of turbulence fluctuations during the fifth half-cycle ($992.74 < t \leqslant 995.88$) and their sudden reappearance during the sixth one, demonstrates the strongly random nature of the flow. However, since when $u_r = 0$ the pressure gradient (2.2) during a half-cycle is opposite to that during the following half-cycle, the ensemble average of the streamwise velocity component must satisfy the equation $\langle u_1(t)\rangle = -\langle u_1(t + T/2)\rangle$. Then, $\langle q(t)\rangle = -\langle q(t + T/2)\rangle$ from which it follows that $\langle q\rangle_{pa} = 0$. We can affirm that for $u_r = 0$ the period average of the ensemble average of q is equal to zero while the period average of q is different from zero and can take both positive and negative values.

An attempt to show that in the present computation $\langle q\rangle_{pa}$ is equal to zero has been made by checking that the series $S_q(n) = (1/n)\sum_{i=1}^{n} q_{pa}(i)$ (see equation (3.2)) tends to zero as the number n of cycles grows. In figure 4(b), after some oscillations of large amplitude, the series S_q attains values close to zero. We feel that the result displayed in figure 4(b) provides sufficient evidence that S_q does tend to zero. An improvement of this result would be possible but a much larger number of cycles would need to be simulated, such that the computation becomes uneconomical. To give an idea of the computational costs of the present simulation, the results shown in figure 4 required about 5 hours of CPU time per cycle on a 3.6 GHz Pentium processor. Since 760 cycles are shown in figure 4, the present simulation took about 3800 hours.

When u_r is increased from 0 to 0.3 the flow characteristics change significantly as can be seen in figure 5, where the time development of the velocity component u_1 at $(x_1,\ x_2,\ x_3) = (2.26,\ 0.28,\ 1.77)$ is shown. Even in this case turbulence appears explosively at the end of the accelerating phase but now the flow shows a remarkable asymmetry between two consecutive half-cycles: the velocity fluctuations are larger when the flow is directed from left to right. The fundamental difference between q_{pa} obtained for $u_r = 0$ (see figure 4a) and that for $u_r = 0.3$ (see figure 6a) is that, apart from a few cycles, the latter is always negative while the former changes sign randomly. The most important consequence of this behaviour is that for $u_r = 0.3$ the steady component of q is different from zero. To show this, in figure 6(b) the series S_q is plotted. For large n the series shows a plateau-like region where only small variations around an average value of about -9.5 can be observed. The steady streaming velocity profile $\overline{u_1}$, shown in figure 7, is evaluated by time averaging u_1 during the time interval $496.71 \leqslant t \leqslant 2325.11$, which includes 291 cycles. The steady

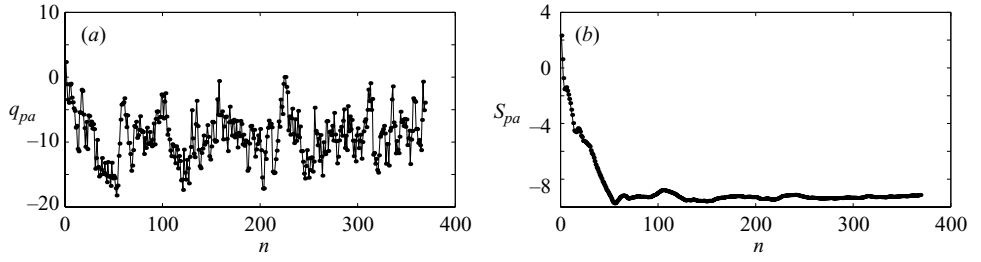

FIGURE 6. (*a*) Period average of the flow rate. (*b*) Trend of the series S_q. $R_\delta = 800$, $u_r = 0.3$.

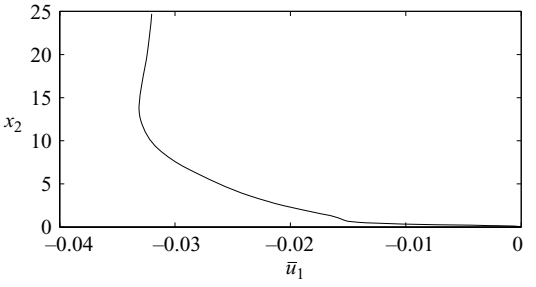

FIGURE 7. Steady component of the streamwise velocity evaluated by time averaging u_1 over the time interval $496.71 \leqslant t \leqslant 2325.11$. $R_\delta = 800$, $u_r = 0.3$.

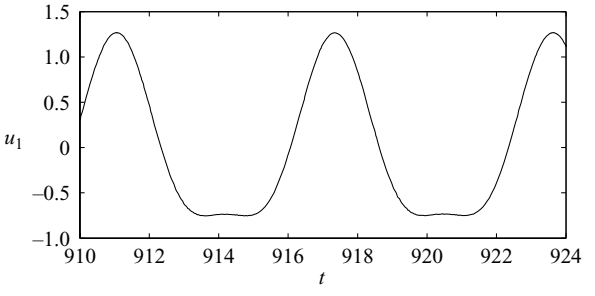

FIGURE 8. Time development of the velocity component u_1 in the irrotational region for $R_\delta = 800$, $u_r = 0.3$.

component of the streamwise velocity clearly persists far from the wall and takes an average value in the x_2-direction which is about 3 % of the velocity amplitude U_0^*. The direction of the steady streaming coincides with that of the smaller amplitude velocity oscillations in the irrotational region (see figure 8), which is offshore in the case of a sea wave bottom boundary layer. In figure 9(*a*) the period average F_{pa} of the dimensionless hydrodynamic force $F = F^*/(\varrho^* U_0^{*2})$ acting per unit area of the plate is shown. The value of F_{pa} changes sign a large number of times during the simulation. The series $S_F(n) = (1/n)\sum_{i=1}^{n} F_{pa}(i)$ is shown in figure 9(*b*). It can be observed that S_F tends to zero when the value of n increases. This result confirms the theoretical finding of § 3 that the steady component of the hydrodynamic force acting on the plate is equal to zero even in the presence of steady streaming.

According to (3.5) the steady component of the streamwise velocity is forced by the period average of the Reynolds stress, therefore it is expected that when the Reynolds number increases the steady component of the flow rate increases as well.

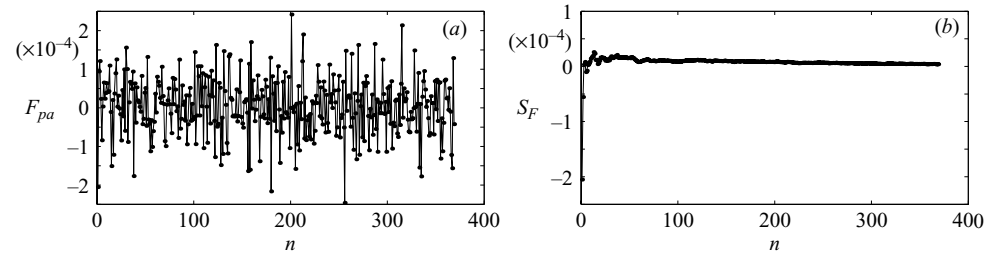

FIGURE 9. (*a*) Period average of the hydrodynamic force acting per unit area of the plate. (*b*) Trend of the series S_F. $R_\delta = 800$, $u_r = 0.3$.

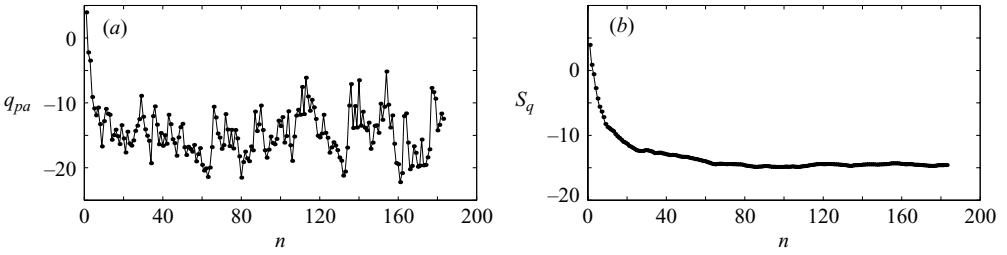

FIGURE 10. (*a*) Period average of the flow rate. (*b*) Trend of the series S_q. $R_\delta = 1000$, $u_r = 0.3$.

To verify this conjecture, a simulation at $R_\delta = 1000$ and $u_r = 0.3$ is performed. The size of the computational domain is fixed as in the previous case, while 120, 120 and 80 gridpoints are introduced in the streamwise, cross-stream and spanwise directions respectively. This computation took about 19 hours of CPU time to perform one cycle on a 3.6 GHz Pentium processor. The whole computation required about 3400 hours.

In figure 10(*a*) it can be observed that the period average of the flow rate is negative for almost all the cycles. Figure 10(*b*) shows that the series S_q converges to a value of about -15, which is larger than the one obtained for $R_\delta = 800$.

Figures 11, 12 and 13 present the mean velocity profiles, the root mean square (r.m.s.) values of the fluctuating velocity components and the Reynolds stress respectively for 16 phases for $R_\delta = 1000$ and $u_r = 0.3$. The mean quantities have been computed by performing spatial averages in the planes $x_2 = \text{const}$ and phase averages over 73 cycles.

In figure 11, where the laminar velocity profiles are also displayed, it can be observed that at the phase $\phi = 0$ the mean velocity profile of the turbulent flow attains its maximum value, then it decreases and reaches the minimum value at $\phi = \pi$. Because of the asymmetry of the pressure gradient that drives the flow, the absolute value of the velocity at $\phi = 0$ is larger than that at $\phi = \pi$. While for $u_r = 0$ there is no difference between the laminar and the turbulent velocity profiles far from the wall, in the present case a small difference can be observed which is equal to about 0.05 at all the phases. This result is due to the presence of negative steady streaming generated by the Reynolds stress.

In agreement with the known results for a steady turbulent channel flow (Kim & Moin 1987), in figure 12 $\langle u_1' u_1' \rangle^{1/2}$ is larger than both $\langle u_2' u_2' \rangle^{1/2}$ and $\langle u_3' u_3' \rangle^{1/2}$. The maximum value of $\langle u_1' u_1' \rangle^{1/2}$ is attained at $\phi = 0$, when the streamwise velocity is maximum, and is equal to about 0.21. The r.m.s. of u_2' and of u_3' are also large at $\phi = 0$ but they tend to grow during the first part of the decelerating phase and they

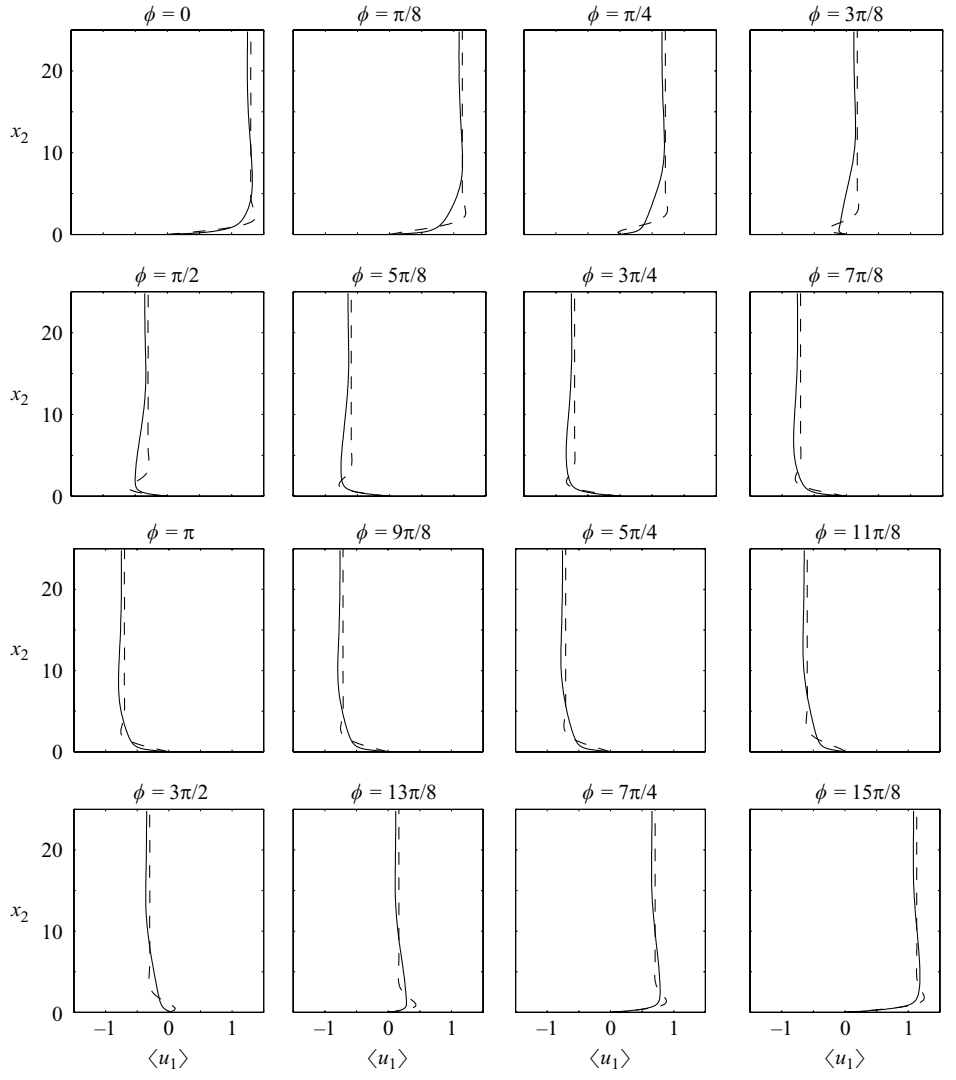

FIGURE 11. Velocity profiles at different phases during the cycle; continuous line: turbulent mean velocity profiles; dashed line: laminar velocity profiles. $R_\delta = 1000$, $u_r = 0.3$.

attain their maximum values, equal to 0.057 and 0.070 respectively, at $\phi = \pi/8$. During the decelerating phase $\langle u_1' u_1' \rangle^{1/2}$ decreases rapidly and at $\phi = \pi/2$ the values of all the r.m.s. do not differ much. From figure 12 it can also be observed that although during the decelerating phase the values of the r.m.s. tend to decay, the turbulence spreads in the vertical direction. During the following accelerating phase ($\pi/2 < \phi < \pi$) the r.m.s. grow again and attain another maximum at about $\phi = 7\pi/8$. The r.m.s. decrease for $\phi > \pi$ and at $\phi = 3\pi/2$ they reach values close to each other as previously observed at $\phi = \pi/2$. Because of the flow asymmetry, the r.m.s. at $\phi = 0$ are different from those at $\phi = \pi$. The ratios between the r.m.s. at $\phi = 0$ and those at $\phi = \pi$, introduced as a measure of the degree of asymmetry, take the values 1.95, 1.38 and 1.35 for the u_1', u_2' and u_3' components respectively. The largest asymmetry is shown by $\langle u_1' u_1' \rangle^{1/2}$ while $\langle u_2' u_2' \rangle^{1/2}$ and $\langle u_3' u_3' \rangle^{1/2}$ are characterized by asymmetries close to each other.

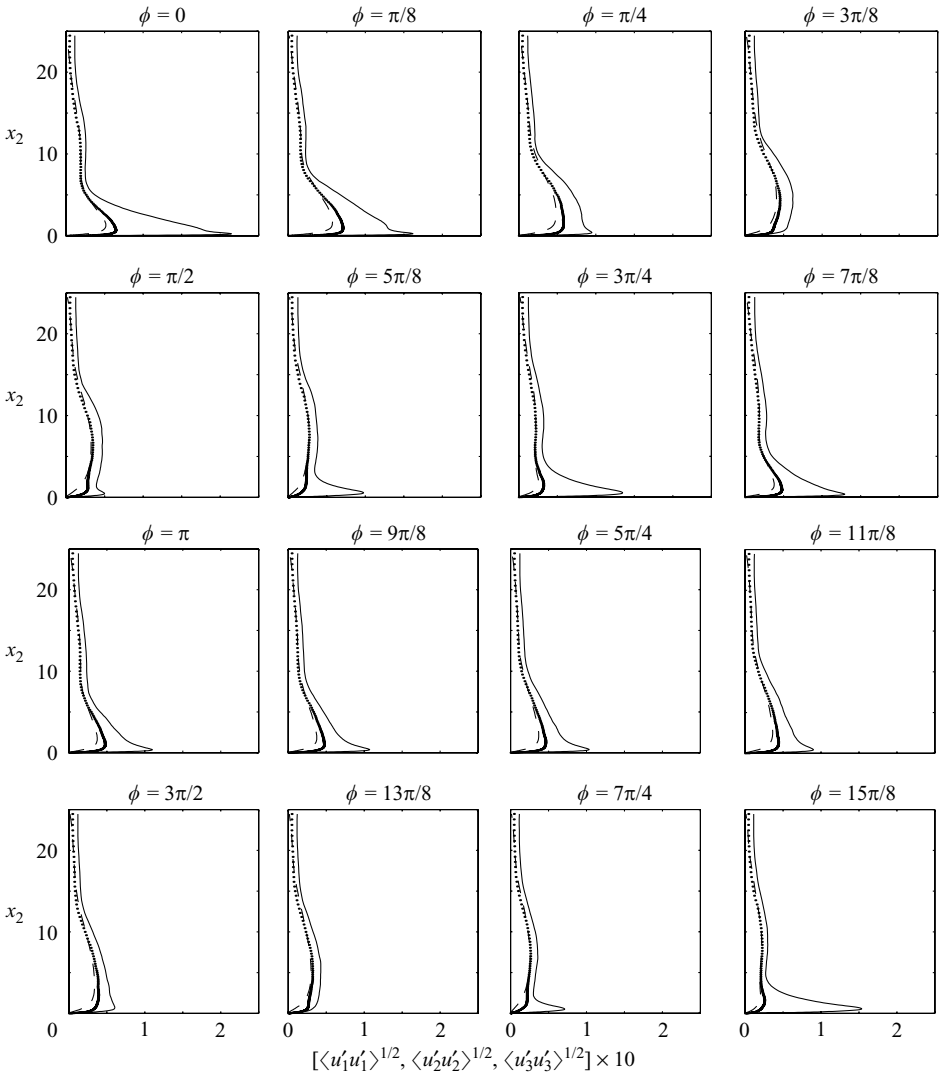

FIGURE 12. Distribution of the r.m.s. of the fluctuating velocity components u_1', u_2' and u_3'; continuous line: $\langle u_1'u_1'\rangle^{1/2}$; dashed line: $\langle u_2'u_2'\rangle^{1/2}$; dots: $\langle u_3'u_3'\rangle^{1/2}$. $R_\delta = 1000$, $u_r = 0.3$.

The asymmetry of the fluctuating velocity components gives rise to an asymmetry in the distribution of the Reynolds stress $\langle u_1'u_2'\rangle$, as can be observed in figure 13. The degree of asymmetry of the Reynolds stress, evaluated according to the previously adopted method, is equal to 2.12. Since the asymmetry of $\langle u_1'u_1'\rangle^{1/2}$ is the largest, the u_1' component should give the largest contribution to the asymmetry of the Reynolds stress.

Although the Reynolds stress distribution during the cycle shows a remarkable asymmetry, its period average is an order of magnitude smaller. In figure 14 $\langle u_1'u_2'\rangle_{pa}$ has values which are an orders of magnitude smaller than the Reynolds stress in the range $0 \leqslant x_2 \leqslant 1$ and two order of magnitude smaller for $x_2 > 1$. The maximum absolute value of $\langle u_1'u_2'\rangle_{pa}$ occurs at $x_2 = 0.2$ and is equal about to 9.2×10^{-5}.

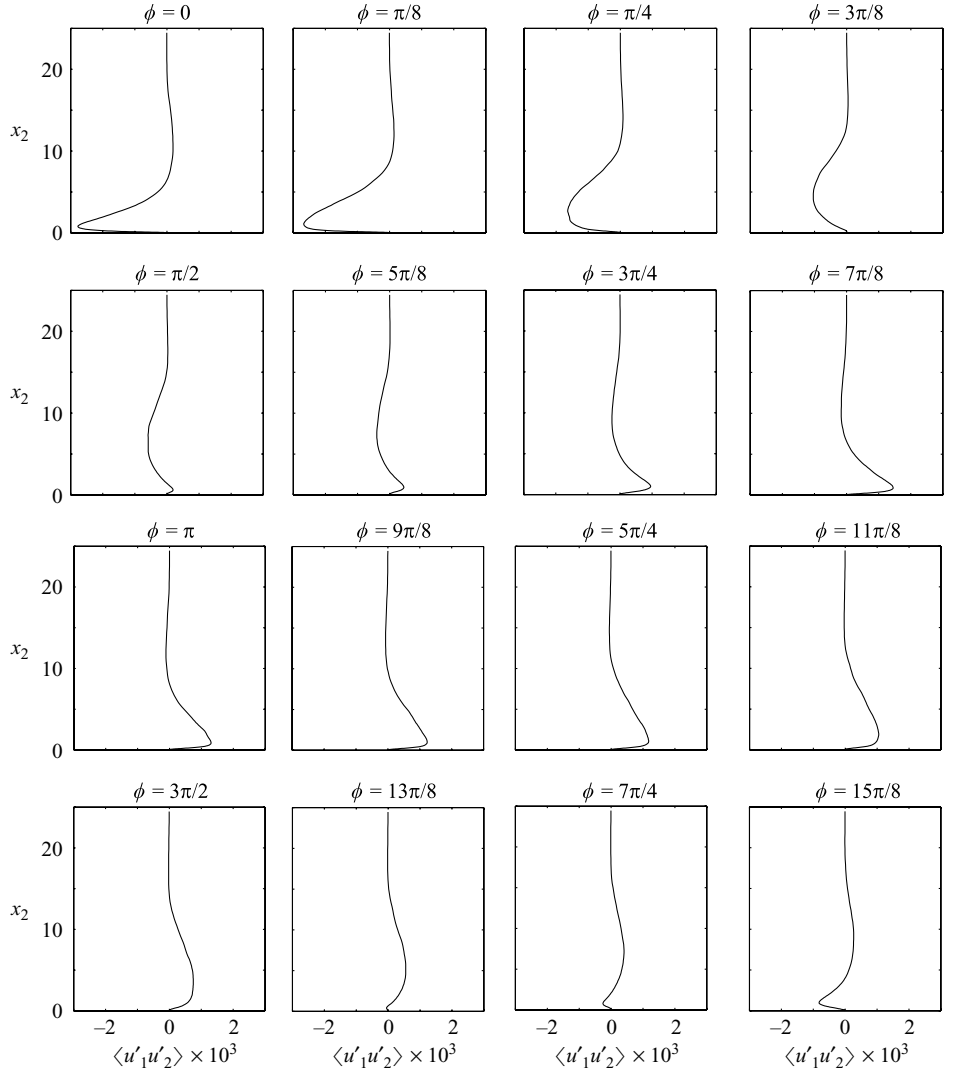

FIGURE 13. Distribution of the Reynolds stress $\langle u'_1 u'_2 \rangle$. $R_\delta = 1000$, $u_r = 0.3$.

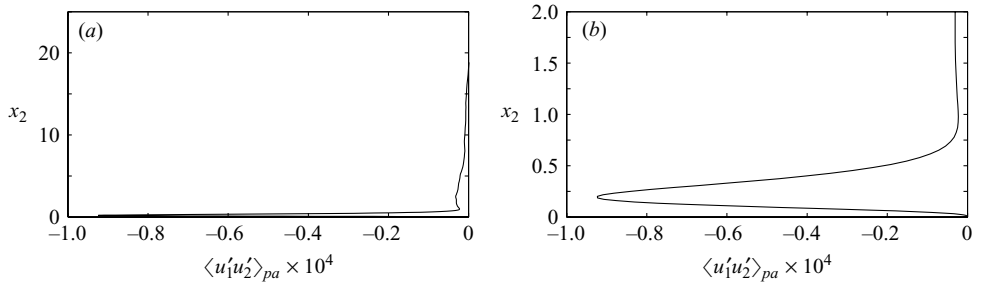

FIGURE 14. (*a*) Steady component of the Reynolds stress. (*b*) Enlarged view of the steady component of the Reynolds stress close to the wall. $R_\delta = 1000$, $u_r = 0.3$.

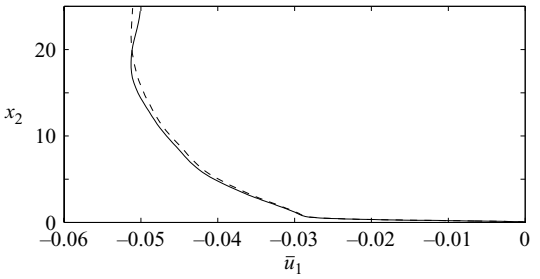

FIGURE 15. Steady component of the streamwise velocity; dashed line: computed by time averaging the streamwise velocity; continuous line: computed by using equation (3.5). $R_\delta = 1000$, $u_r = 0.3$.

Apart from averaging the velocity u_1, the steady streaming velocity profile $\overline{u_1}$ can be evaluated by another procedure, i.e. by computing first the period average of the Reynolds stress $\langle u_1' u_2' \rangle_{pa}$ and then using equation (3.5). However, as both $\overline{u_1}$ and $\langle u_1' u_2' \rangle_{pa}$ are evaluated by performing a time average over a finite number of cycles, it cannot be expected that the two procedures provide exactly the same result because they hold rigorously only when the number of cycles tends to infinity. The results plotted in figure 14 show that the steady streaming is generated by a negative balance of the Reynolds stress during the cycle, which should be largely due to the explosive development of turbulence around the end of the accelerating phase. By introducing in equation (3.5) the Reynolds stresses reported in figure 14, we have obtained the velocity profile $\overline{u_1}$ shown in figure 15, where the velocity profile obtained by time averaging the velocity component u_1 is also displayed. It can be observed that the two results are in a fair agreement. The spatial average in the x_2-direction of the steady streaming velocity is 4–5 % of U_0^* and is in reasonable agreement with the experimental results of Ribberink & Al-Salem (1995) who performed an asymmetric oscillatory flow experiment in a water tunnel for R_δ and u_r equal to about 10^3 and 0.3 respectively. Because of mass conservation, in the central part of the tunnel a return flow was present which balanced the flow due to the steady streaming close to the walls. Unfortunately, this phenomenon does not allow a quantitative comparison between the experiments of Ribberink & Al-Salem (1995) and present results as the return flow strongly altered the velocity profile of the steady streaming. Moreover, Ribberink & Al-Salem (1995) did not perform measurements sufficiently close to the wall: by looking at figure 4 of their paper it can be observed that the first measurement point is placed at about $14\delta^*$ which is too far from the wall.

5. Conclusions

The present study deals with the steady streaming generated in a spatially uniform turbulent boundary layer driven by a purely oscillating pressure gradient. The main results of the study can be summarized as follows:

(i) when the flow is forced by a sinusoidal oscillating pressure gradient, no steady streaming is generated;

(ii) when the flow is generated by a pressure gradient given by the sum of two sinusoidal functions, characterized by angular frequencies ω_1 and $\omega_2 = 2\omega_1$, steady streaming is generated within the boundary layer and it persists in the irrotational region.

The generation of the steady streaming is due to non-vanishing values of the period average of the Reynolds stress. If the integral of this quantity along the x_2-direction is negative the steady streaming is also negative, otherwise it is positive. It is shown both theoretically and numerically that the steady component of the hydrodynamic force acting on the plate vanishes even when a steady current is present. The numerical simulations show that the steady streaming has the same direction as the smaller amplitude velocity oscillations in the irrotational region. This result is due to the larger absolute value of the Reynolds stress that develops when the flow direction is the same as the larger velocity amplitude. In a sea wave bottom boundary layer, the direction of the smaller velocity amplitude is offshore, so that the direction of the asymmetry-wave steady streaming is also offshore. Moreover, in this case, the Longuet-Higgins steady streaming, which acts in the onshore direction, is also present. As the Longuet-Higgins steady streaming has not been included in this study, on the basis of the present results we cannot draw definitive conclusions about the direction and the strength of the steady streaming for a wave-induced turbulent boundary layer. A possible development of the present work is studying the asymmetry-wave steady streaming in the fully developed turbulent regime which characterizes the wave boundary layer at high Reynolds numbers. Moreover, in order to improve knowledge of the hydrodynamics of real sea wave bottom boundary layers, the Longuet-Higgins steady streaming should also be considered in future works on this subject.

REFERENCES

Akhavan, R., Kamm, R. D. & Shapiro, A. H. 1991*a* An investigation of transition to turbulence in bounded oscillatory Stokes flow. Part 1. Experiments. *J. Fluid Mech.* **225**, 395–422.

Akhavan, R., Kamm, R. D. & Shapiro, A. H. 1991*b* An investigation of transition to turbulence in bounded oscillatory Stokes flow. Part 2. Numerical simulations. *J. Fluid Mech.* **225**, 423–444.

Bijker, E. W., Kalkwijk, J. P. T. & Picters, T. 1974 Mass transport in gravity waves on a sloping bottom. In *Proc.* 14th *Coastal Engng Conf*., pp. 447–465. ASCE.

Blennerhassett, P. J. & Bassom, A. P. 2006 The linear stability of high-frequency oscillatory flow in a channel. *J. Fluid Mech.* **556**, 1–25.

Brebner, A., Askew, J. A. & Law, S. W. 1966 The effect of roughness on the mass-transport of progressive gravity waves. In *Proc.* 10th *Coastal Engng Conf*., pp. 175–184. ASCE.

Costamagna, P., Vittori, G. & Blondeaux, P. 2003 Coherent structures in oscillatory boundary layers. *J. Fluid Mech.* **474**, 1–33.

Cowley, S. J. 1987 High frequency Rayleigh instability of Stokes layers. In *Stability of Time Dependent and Spatially Varying Flows* (ed. D. L. Dwayee & M. Y. Hussaini), pp. 261–275. Springer.

Dean, R. G. & Dalrymple, R. A. 2000 *Water Wave Mechanics for Engineers and Scientists*. World Scientific.

Eckmann, D. M. & Grotberg, J. B. 1991 Experiments on transition to turbulence in oscillatory pipe flow. *J. Fluid Mech.* **222**, 329–350.

Hall, P. 1978 The linear stability of flat Stokes layers. *Proc. R. Soc. Lond.* A **359**, 151–166.

Hall, P. 2003 On the stability of Stokes layers at high Reynolds numbers. *J. Fluid Mech.* **482**, 1–15.

Hino, M., Kashiwayanagi, M., Nakayama, A. & Hara, T. 1983 Experiments on the turbulence statistics and on the structure of a reciprocating oscillatory flow. *J. Fluid Mech.* **131**, 363–400.

Hino, M., Sawamoto, M. & Takasu, S. 1976 Experiments on transition to turbulence in an oscillatory pipe flow. *J. Fluid Mech.* **75**, 193–207.

Jacobs, S. J. 1984 Mass transport in a turbulent boundary layer under a progressive water wave. *J. Fluid Mech.* **146**, 303–312.

Jensen, B. L., Sumer, B. M. & Fredsøe, J. 1989 Turbulent oscillatory boundary layers at high Reynolds numbers. *J. Fluid Mech.* **206**, 265–297.

von Kerczek, C. & Davis, S. H. 1974 Linear stability theory of oscillatory Stokes layers. *J. Fluid Mech.* **62**, 753–773.

Kim, J. & Moin, P. 1985 Application of a fractional step method to incompressible Navier–Stokes equations. *J. Comput. Phys.* **59**, 308–323.

Kim, J. & Moin, P. 1987 Turbulent statistics in fully developed channel flow at low Reynolds number. *J. Fluid Mech.* **177**, 133–166.

Lodahl, C. R., Sumer, B. M. & Fredsøe, J. 1998 Turbulent combined oscillatory flow and current in a pipe. *J. Fluid Mech.* **373**, 313–348.

Longuet-Higgins, M. S. 1953 Mass transport in water waves. *Phil. Trans. R. Soc. Lond.* A **345**, 535–581.

Longuet-Higgins, M. S. 1958 The mechanics of the boundary layer near the bottom in a progressive wave. Appendix to "An experimental investigation of drift profiles in a closed channel" by R. C. H. Russel and D. C. Osorio. In *Proc.* 6th *Coastal Engng Conf.*, p. 171. ASCE.

Monin, A. S. & Yaglom, A. M. 1971 *Statistical Fluid Mechanics: Mechanics of Turbulence, Vol. 1*. The MIT Press.

Rai, M. M. & Moin, P. 1991 Direct simulation of turbulent flow using finite-difference schemes. *J. Comput. Phys.* **96**, 15–53.

Rayleigh, Lord 1883 On the circulation of air observed in Kundt's tubes and some allied acoustical problems. *Phil. Trans. R. Soc. Lond.* A **175**, 1–21.

Ribberink, J. S. & Al-Salem, A. A. 1995 Sheet flow and suspension of sand in oscillatory boundary layers. *Coastal Engng* **25**, 205–225.

Riley, N. 2001 Steady streaming. *Annu. Review Fluid Mech.* **33**, 43–65.

Russel, R. C. H. & Osorio, J. D. C. 1958 An experimental investigation of drift profiles in a closed channel. In *Proc.* 6th *Coastal Engng Conf.*, p. 171. ASCE.

Spalart, P. R. & Baldwin, B. S. 1987 Direct simulation of a turbulent oscillating boundary layer. In 6th *Symp. on Turbulent Shear flows, Tolouse* 7–9 Sept. (ed. F. Durst, B. Launder, F. Schmidt & J. Whitelaw), pp. 417–440.

Stokes, G. G. 1851 On the effect of internal friction of fluids on the motion of pendulums. *Trans. Camb. Phil. Soc.* **9**, 8–106.

Trowbridge, J. & Madsen, O. S. 1984 Turbulent wave boundary layers 2. Second-order theory and mass transport. *J. Geophys. Res.* **89**(5), 7999–8007.

Van Doorn, T. 1981 Experimental investigation of near-bottom velocities in water waves with and without a current. *Tech. Rep.* M1423. Delft Hydraulics.

Vittori, G. & Verzicco, R. 1998 Direct simulation of transition in an oscillatory boundary layer. *J. Fluid Mech.* **371**, 207–232.

Wu, X. 1992 The nonlinear evolution of high-frequency resonant triad waves in an oscillatory Stokes layer at high Reynolds number. *J. Fluid Mech.* **245**, 553–597.